

# Fast Charging All Solid-State Lithium Batteries Enabled by Rational Design of Dual Vertically-Aligned Electrodes

Xuejie Gao, Xiaofei Yang, Keegan Adair, Jianneng Liang, Qian Sun, Yang Zhao, Ruying Li, Tsun-Kong Sham,\* and Xueliang Sun\*

The slow charging limitations of all-solid-state lithium batteries (ASSLBs) have significantly limited their practical application. Thus, significant improvement of the rate performance and development of fast charging ASSLBs is crucial for the commercialization of these systems. However, poor  $\text{Li}^+$  transport kinetics and Li dendrite formation under high charging current densities have inhibited their capabilities. To tackle these issues, the design of dual vertically-aligned electrodes (DVAEs) is proposed to accelerate  $\text{Li}^+$  transport and suppress Li dendrite formation. At the anode side, the vertically-aligned Li (VA-Li) anode with lithiophilic micro-walls enables lateral growth of Li deposits rather than perpendicular to the electrode surface, thus preventing dendrite penetration through the separator. In addition, the 3D vertically-aligned structure in both VA-Li and vertically-aligned- $\text{LiFePO}_4$  (VA-LFP) enables enhanced  $\text{Li}^+$  transport due to lower tortuosity and faster  $\text{Li}^+$  transport kinetics. Benefitting from the rational design, VA-Li symmetric cells can operate for 300 h at a current density/capacity of  $3 \text{ mA cm}^{-2}/3 \text{ mAh cm}^{-2}$ , while short-circuiting is observed after 87 h for bare Li cycled at only  $0.5 \text{ mA cm}^{-2}$  (capacity:  $0.5 \text{ mAh cm}^{-2}$ ). Moreover, a fast-charging ASSLBs assembled with DVAEs demonstrates a high capacity of  $89.4 \text{ mAh g}^{-1}$  after 2000 cycles at 4C.

properties, low cost and scalable fabrication methods.<sup>[2]</sup> Nevertheless, many of the recently reported SPE-based ASSLBs can only operate at current densities/areal capacities lower than  $0.5 \text{ mA cm}^{-2}/0.5 \text{ mAh cm}^{-2}$ , which is far below the requirements for commercialization.<sup>[3]</sup> The low operating current densities prevent these ASSLBs from being used in fast charging applications such as electric vehicles. Therefore, it is imperative to design electrode structures which can improve the operating current density and realize fast charging ASSLBs.

In general, the working current density in ASSLBs is limited by several factors: 1) The ionic conductivity of SPE; 2) Li dendrite growth; 3)  $\text{Li}^+$  transport in the electrode.<sup>[4]</sup> To improve the ionic conductivity, several inorganic fillers (metal oxides, oxide- and sulfide solid-state electrolytes (SSEs)), plasticizers (succinonitrile (SN)), and low molecular weight poly (ethylene glycol) dimethyl ether, starch) have been developed and demonstrated to be effective in achieving high ionic conductivities

of  $10^{-5}$ – $10^{-4}$  at room temperature (RT). Moreover, for suppressing Li dendrite growth in SPE-based ASSLBs, inorganic fillers, cross-linking structures, and electrolyte additives have proven to be effective.<sup>[5]</sup> The first two strategies play important roles in enhancing the mechanical strength of the SPE, while the latter aims to promote uniform Li nucleation. For instance, our group showed that a glass fiber scaffold can prolong the cycling life of Li–Li symmetric cells to over 2000 h at a current density of  $0.2 \text{ mA cm}^{-2}$  (capacity:  $0.2 \text{ mAh cm}^{-2}$ ).<sup>[6]</sup> In another case, Armand's group extended the cycling life of Li–Li symmetric cells by sixfold at a current density of  $0.1 \text{ mA cm}^{-2}$  (capacity:  $0.2 \text{ mAh cm}^{-2}$ ) with the introduction of a  $\text{LiN}_3$  additive.<sup>[7]</sup> Despite the great achievements made in improving ionic conductivity and dendrite suppression, fast charging SPE-based ASSLBs have rarely been reported.

In most cases, planar Li is directly used as the Li anode, which has a low geometric surface area and results in high overpotential and serious Li dendrite growth during plating under high current densities.<sup>[8]</sup> It should be noted that the Li dendrite growth direction is perpendicular to Li anode, increasing the risk of dendrites penetrating the SPEs.<sup>[9]</sup> Moreover, the cathodes obtained by conventional blade casting relatively dense structures and  $\text{Li}^+$  transport channels with high


## 1. Introduction

As promising next-generation energy storage systems beyond the state-of-the-art Li-ion batteries, all-solid-state lithium batteries (ASSLBs) have received considerable attention due to their improved safety and energy density.<sup>[1]</sup> Among the various ASSLB systems, solid polymer electrolytes (SPEs) have been regarded as one of the most promising candidates for practical application due to their chemical/electrochemical stability, mechanical

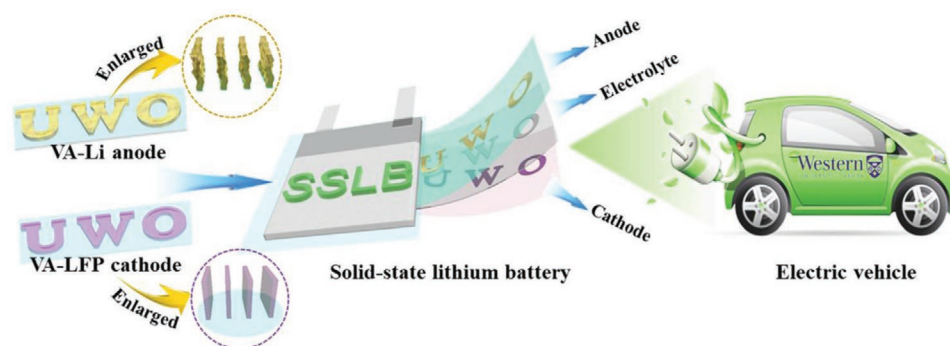
X. Gao, Dr. X. Yang, K. Adair, J. Liang, Dr. Q. Sun, Dr. Y. Zhao, R. Li, Prof. X. Sun

Department of Mechanical and Materials Engineering  
University of Western Ontario  
London, Ontario N6A 5B9, Canada  
E-mail: xsun9@uwo.ca

X. Gao, Prof. T.-K. Sham  
Department of Chemistry  
University of Western Ontario  
London, Ontario N6A 5B7, Canada  
E-mail: tsham@uwo.ca

 The ORCID identification number(s) for the author(s) of this article can be found under <https://doi.org/10.1002/adfm.202005357>.

DOI: 10.1002/adfm.202005357



**Scheme 1.** Schematic illustration of the fabrication process of the VA-Li anode and the VA-LFP cathode with SPEs for all solid-state Li batteries.

tortuosity, which hinders the  $\text{Li}^+$  transport in the electrode and rate performance.<sup>[10]</sup> With this in mind, a strategy to concurrently suppress the Li dendrite growth and reduce the tortuosity of electrodes is required for fast charging ASSLB.

Herein, a dual vertically-aligned electrode (DVAE) configuration with well-controlled microscale features is proposed to promote the development of fast charging ASSLBs. During plating, Li selectively nucleates and grows within the micro-channel walls of the vertically-aligned Li anode (VA-Li), which reduces the local current density as well as changes the Li growth direction from perpendicular to parallel. The confinement of Li nucleation is beneficial toward suppressing Li dendrite growth and reducing the risk of short-circuiting under high current densities. To minimize the  $\text{Li}^+$  transport tortuosity in both the anode and cathode, a vertically-aligned  $\text{LiFePO}_4$  (LFP) is designed to facilitate  $\text{Li}^+$  transport and reduce  $\text{Li}^+$  diffusion resistance, thus improving the rate performance. Based on the DVAE structure, both fast charging SPE-based Li-Li symmetric cells and Li-LFP full cells are realized. The Li-Li symmetric cells achieve excellent cycling performance for over 300 h under ultrahigh current densities/areal capacities of  $3 \text{ mA cm}^{-2}/3 \text{ mAh cm}^{-2}$  with a low overpotential of around 100 mV. More importantly, the Li-LFP ASSLBs demonstrate ultra-long cycling life of over 2000 cycles under a high current density of 4C with a high discharge capacity of  $120 \text{ mAh g}^{-1}$ . Insights gained from this work will open up new opportunities for the development of fast charging ASSLBs.

## 2. Results and Discussion

The design of the ASSLBs with DVAE structure can be seen in **Scheme 1**, where a SPE is sandwiched between VA-Li and VA-LFP electrodes. During charging, the  $\text{Li}^+$  is rapidly moved out from LFP through the vertically-aligned channels. After diffusion of  $\text{Li}^+$  to the anode, it will selectively nucleate on the lithiophilic micro-walls with ZnO coating. Based on the orientation of the microchannels, the Li growth direction changes from perpendicular to the electrode surface to parallel, which significantly reduces the risk of Li penetration through the SPE. Moreover, the micro-walls possess a large specific surface area, which provides a large number of Li nucleation sites and greatly reduces the local current density. At the same time, the vertically-aligned channels among the micro walls supply a

large space for Li accommodation and enables fast Li transport due to the reduced tortuosity. In this regard, we can deduce that the as-designed VA-Li anode can meet the requirements of  $\text{Li}^+$  transport and Li dendrite suppression during fast charging. During the subsequent discharging process, at the anode side, the Li metal will be oxidized into  $\text{Li}^+$  and transport through the vertically-aligned channels back to the cathode. At the cathode side, the  $\text{Li}^+$  undergoes diffusion into the LFP structure. Benefitting from the well-designed DVAE structure, fast charging ASSLBs may be realized.

The morphology of the DVAE structure is characterized by scanning electron microscopy (SEM). As shown in **Figure 1a**, the VA-LFP is firstly fabricated with a 3D-printer combined with a freeze-drying technique. Based on the anisotropic crystal growth kinetics, the lamellar ice acts as an in-situ formed template and transforms the LFP electrode into the VA-LFP with numerous vertically-aligned micro-walls (thickness:  $\approx 12 \mu\text{m}$ , **Figure 1b,c**).<sup>[11]</sup> Among the micro-walls are vertically-aligned channels with a thickness of around  $35 \mu\text{m}$  (**Figure 1d-h**). Compared with a conventional blade-casted LFP cathode (**Figure S1**, Supporting Information), the VA-LFP cathode provides more  $\text{Li}^+$  transport channels with reduced tortuosity, thus facilitating  $\text{Li}^+$  transport during cycling. For VA-Li fabrication, a similar process is firstly used to obtain a vertically-aligned carbon nanotube (CNT)-based Li host (labeled as VA-Li host, **Figure S2a,c-g**, Supporting Information), where the CNTs are coated with a thin layer of ZnO (**Figure S2b**, Supporting Information). The ZnO acts as a lithiophilic coating on the micro-walls and promotes Li infusion into the vertically-aligned scaffold upon contact with molten Li.<sup>[12]</sup> As can be seen in **Figure S3** (Supporting Information), the molten Li shows a strong affinity toward the host and can easily infuse into the vertically-aligned structure. The electrodes are completely infused with Li metal after  $\approx 14 \text{ s}$ . After infiltration of Li, the black VA-Li host turns to gold with a metallic Li luster. The morphology evolution at the micro-level is further characterized by SEM. As shown in **Figure 1j,k**, the micro-walls are broadened (from 12 to  $22 \mu\text{m}$ ) and the micro-channels narrowed ( $35$  to  $28 \mu\text{m}$ ), further confirming that Li is successfully infused into the vertically-aligned scaffold. It should be mentioned that the available void space between the micro-channels is critical toward accelerating  $\text{Li}^+$  transport as well as Li accommodation during Li plating. With this in mind,

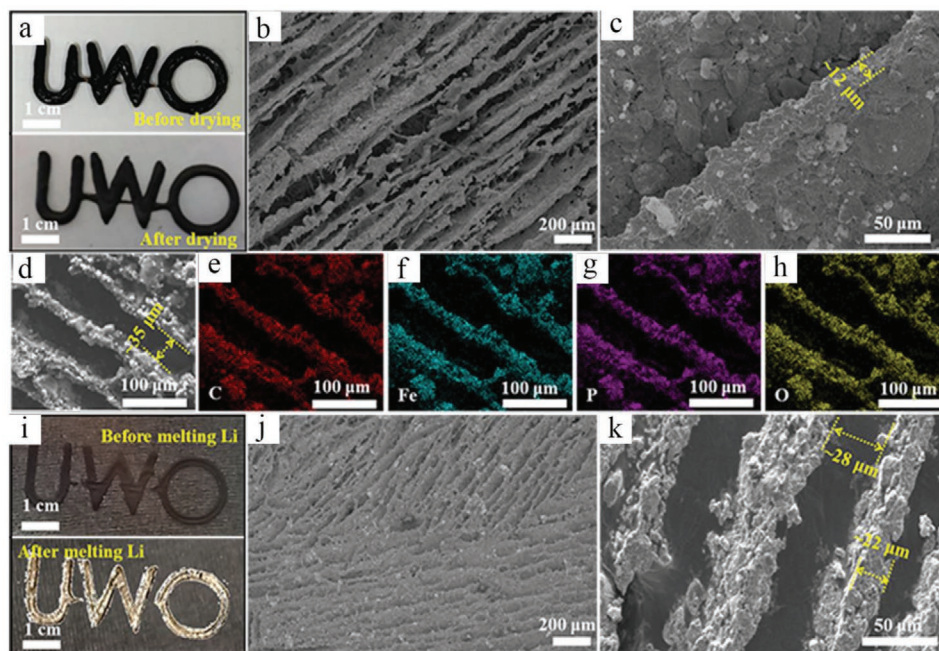


**Figure 1.** Morphologies of the VA-Li anode and VA-LFP cathode a) Optical images of the VA-LFP before and after drying. b–h) Surface SEM images and corresponding elemental mappings of the VA-LFP cathode at different magnifications. i) Optical images of the VA-Li host before and after melting Li. j, k) Surface SEM images of the VA-Li at different magnifications.

the unique DVAE structure is expected to enhance Li dendrite suppression and facilitate  $\text{Li}^+$  transport at high current densities.

The important role of VA-Li in suppressing Li dendrite formation is investigated by Li–Li symmetric cells, where bare Li is chosen for comparison. **Figure 2a–d** displays the schematic representation of the Li deposition behavior in the Li–Li symmetric cells and relevant Li symmetrical cell performance using VA-Li and bare Li electrodes. As illustrated in **Figure 2a**, benefiting from the vertically-aligned micro-walls that direct uniform lithium deposition within the microchannels, the VA-Li symmetric cells exhibit lower overpotentials compared to the cells containing bare Li (**Figure 2b,c**). For instance, as shown in **Figure 2b**, at a current density of  $0.2 \text{ mA cm}^{-2}$  ( $0.2 \text{ mAh cm}^{-2}$ ), the overpotential of VA-Li symmetric cell is around 8 mV, which is a small fraction of its counterpart (bare Li:  $\approx 130 \text{ mV}$ ). Moreover, the VA-Li symmetric cell also demonstrates more stable cycling performance than the bare Li (**Figure 2b,c**). Even after 1500 h, the overpotential shows negligible change and delivers a value of around 10 mV, indicating a stable Li plating/stripping process (**Figure 2b**). The inherent stability and low overpotentials of the VA-Li electrode can be attributed to the high surface area provided by the vertically aligned channels, where the lithophilic micro-channel walls guide Li nucleation and growth in a parallel direction instead of perpendicular to the electrode surface (**Figure 2a**). The confinement of Li within the microchannels prevents Li dendrites from penetrating the separator, leading to prolonged cycle life with improved safety. In contrast, for the bare Li symmetric cells, large fluctuations in the plating/stripping profiles are observed after 270 h and the overpotential suddenly drops to nearly 0 V after 320 h, indicating the occurrence of short-circuiting. Moreover, the Li

dendrite suppression capability of VA-Li is further studied at an elevated current density/capacity of  $0.5 \text{ mA cm}^{-2}/0.5 \text{ mAh cm}^{-2}$  (**Figure 2c**). As expected, the VA-Li still displays stable plating/stripping behavior, with a relatively low overpotential around 24 mV after 650 h (**Figure 2c** and **Figure S4**, Supporting Information). On the contrary, the occurrence of hard short-circuits is observed in the bare Li cell after 87 h.

According to the Cui's and Deng's simulation, a charge rate of 3.2C is required to meet the demand of fast-charging lithium batteries in electric vehicles, which is equivalent to charging to 80% state of charge (SOC) within 15 min.<sup>[10,13]</sup> Taking a widely used LFP loading of  $5 \text{ mg cm}^{-2}$  (in recently reported SPE-based ASSLBs) into consideration, a current density of  $2.72 \text{ mA cm}^{-2}$  is necessary. With this in mind, a current density of  $3 \text{ mA cm}^{-2}$  (areal capacity:  $3 \text{ mAh cm}^{-2}$ ) is chosen to determine whether our designed VA-Li can achieve the fast charging goal. Promisingly, as displayed in **Figure 2d**, the VA-Li electrode shows stable plating/stripping performance for over 300 h with a low overpotential of around 100 mV (**Figure S5**, Supporting Information). There is no doubt that such excellent performance is superior to recent publications in terms of operating current density and areal capacity listed in **Figure 2e** and **Table S1** (Supporting Information). Overall, the as-designed VA-Li demonstrated excellent Li dendrite suppression under high operating current densities, which will pave the way for the development of fast charging ASSLBs.

To clarify the Li deposition behavior in the VA-Li electrode, the morphology of the VA-Li electrode at different stages of plating is observed by SEM (current density is controlled as  $0.5 \text{ mA cm}^{-2}$ ).<sup>[14]</sup> Before SEM analysis, both bare Li and VA-Li symmetric cells are disassembled and then soaked in a DME solution for 12 h to remove the SPEs. As shown in **Figure 3a–d**,

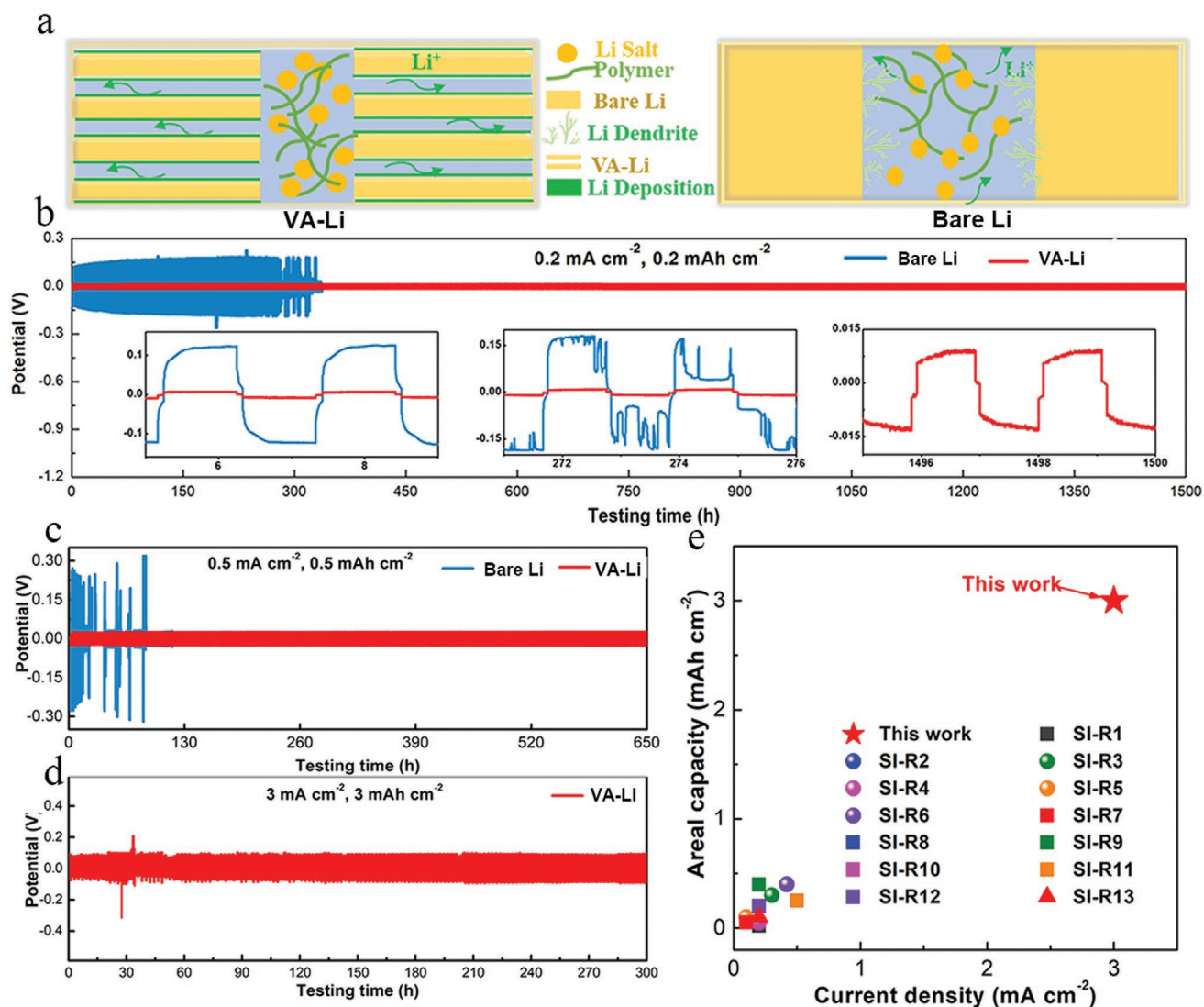


**Figure 2.** Illustration and cycling stability of bare Li and VA-Li symmetric cells with SPEs. a) Schematic of VA-Li (left) symmetric cell and bare Li (right) symmetric cell with SPE. b) VA-Li and bare Li symmetric cells cycled at a current density of  $0.2 \text{ mA cm}^{-2}$  and  $0.2 \text{ mAh cm}^{-2}$ , c)  $0.5 \text{ mA cm}^{-2}$ ,  $0.5 \text{ mAh cm}^{-2}$ , and d)  $3 \text{ mA cm}^{-2}$ ,  $3 \text{ mAh cm}^{-2}$ . e) Comparison of this work with other lithium symmetric cells with SPE from literature.

due to the lithiophilicity of the micro-walls in VA-Li, Li selectively nucleates and gradually fills the vertically-aligned channels. The vertically-aligned channels function as a void space for Li accommodation during electrochemical plating. Even at a high Li plating capacity of  $3 \text{ mAh cm}^{-2}$ , where the vertically-aligned channels are almost filled, no obvious dendrites can be observed. Moreover, the VA-Li symmetric cell operating at a current density of  $0.5 \text{ mA cm}^{-2}$  (areal capacity:  $0.5 \text{ mAh cm}^{-2}$ ) after 50 cycles is disassembled and the surface morphology of VA-Li is checked by SEM. As shown in Figure S6a,b (Supporting Information), the vertically-aligned structure is well-maintained during cycling, demonstrating the stability of the structure and high reversibility of Li plating/stripping process in VA-Li. On the contrary, for bare Li, a rough surface with non-uniform Li deposition and undesirable Li dendrite growth are clearly observed during Li plating, as shown in Figure 3e–h. When the capacity

increases to  $3 \text{ mAh cm}^{-2}$ , some cellulose fibers are observed on the surface of Li anode, indicating that the Li dendrites have pierced through the SPE (Figure S7, Supporting Information). The formation of dendrites is further confirmed by the Li plating profile shown in Figure S8 (Supporting Information). During plating, when the capacity increases to  $1.3 \text{ mAh cm}^{-2}$ , a sharp drop in overpotential is observed, which is associated with short-circuiting. Similar to VA-Li symmetric cells, the morphology of bare Li in a Li–Li symmetric cell after 50 cycles (current density:  $0.5 \text{ mA cm}^{-2}$ , areal capacity:  $0.5 \text{ mAh cm}^{-2}$ ) is also observed by SEM for comparison. As displayed in Figure S6c,d (Supporting Information), numerous cellulose fibers are observed on the Li anode surface. It can be attributed to Li dendrite growth through the cellulose separator. The significant difference in Li deposition behavior within the VA-Li and bare Li electrodes is illustrated in Figure 3a–h. Compared

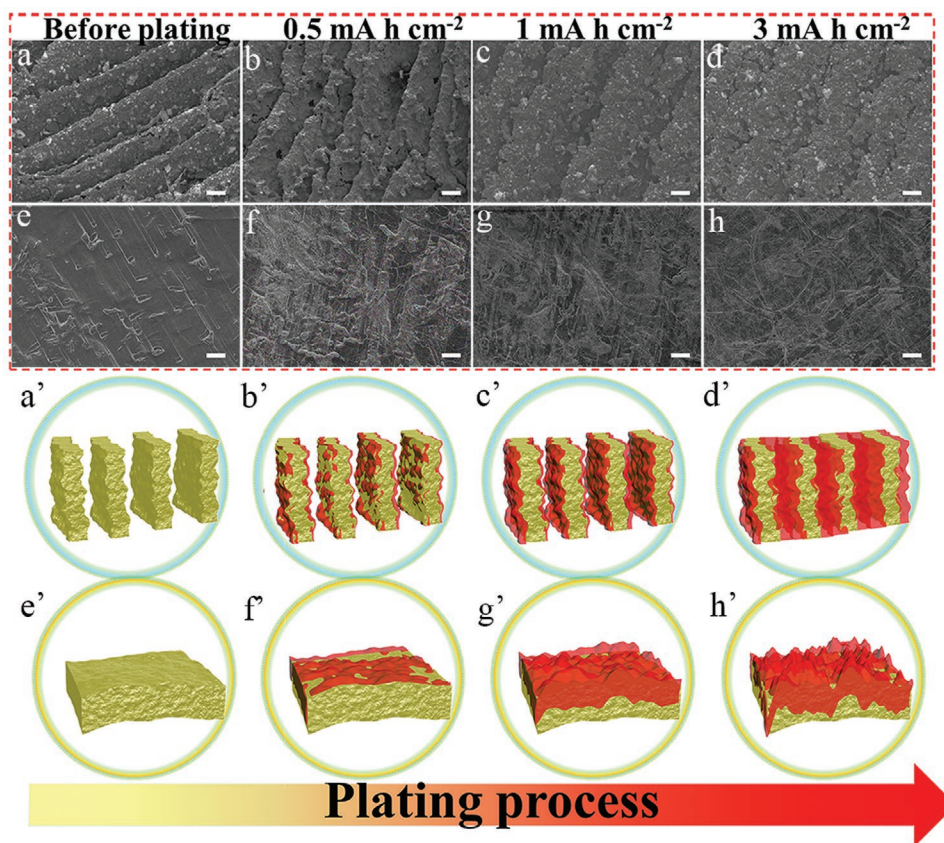


**Figure 3.** a,e) SEM images of surface morphology evolution of VA-Li and bare Li anode before, and after b,f)  $0.5 \text{ mA h cm}^{-2}$ , c,g)  $1 \text{ mA h cm}^{-2}$ , d,h)  $3 \text{ mA h cm}^{-2}$  of Li deposition at a current density  $0.5 \text{ mA cm}^{-2}$  (scale bar:  $50 \mu\text{m}$ ). Schematic illustration of the lithium plating process of a'–d') VA-Li and e'–h') Li, corresponding well with SEM images of surface morphology evolution, from the capacities of  $0.5 \text{ mA h cm}^{-2}$  to  $3 \text{ mA h cm}^{-2}$  at a current density of  $0.5 \text{ mA cm}^{-2}$ .

with the non-uniform Li nucleation and growth found on bare Li, the uniform Li nucleation on the micro-walls and Li confinement within the vertically-aligned channels of VA-Li is the root cause for the improved Li dendrite suppression under high operating current densities.

To investigate the potential application of the VA-Li anode in fast charging ASSLBs, the electrochemical performance of LFP/VA-Li (Figure S9a, Supporting Information) is studied, where the LFP is fabricated by a conventional blade casting method. For comparison, bare Li is chosen as its counterpart and the assembled cell is labeled as LFP/Li (Figure S9b, Supporting Information). Figure 4b shows the rate-performance of LFP/VA-Li and LFP/Li cells under different rates from 0.5 to 4C in the voltage window of 2.5–4.2 V. Generally, the LFP/VA-Li cell delivers higher capacities at all C-rates than that of the LFP/Li cell. Even at a high rate of 4C, a high capacity of  $88 \text{ mAh g}^{-1}$  is still maintained for the LFP/VA-Li cell, while the LFP/Li cell only delivers a capacity of  $\approx 64 \text{ mAh g}^{-1}$  at 2C. The improved rate performance can be attributed to the fast  $\text{Li}^+$  transport in the vertically-aligned channels with low tortuosity in VA-Li. Moreover, it should be noted that a Coulombic efficiency (CE) drop is observed for the LFP/Li cell when the rate is over 3C. The high current densities result in short-circuiting, which is confirmed by the charging/discharging profiles in

Figure S10 (Supporting Information). The difference in rate performance between LFP/VA-Li and LFP/Li proves the merits of VA-Li in enhancing  $\text{Li}^+$  transport and Li dendrite suppression, which coincides well with the electrochemical performance of Li–Li symmetric cells. However, fast ion transport kinetics at the anode satisfies only part of the requirements for fast charging ASSLBs. The rational design of cathode structure also plays a critical role in achieving high rate performance. However, for the LFP cathode obtained by conventional blade casting technique, a dense structure is present (Figure S1, Supporting Information) which inhibits  $\text{Li}^+$  diffusion through the bulk of the electrode. Herein, a DVAE cell design (labeled as VA-LFP/VA-Li, seen in Figure 4a) is fabricated with another VA-LFP to further facilitate  $\text{Li}^+$  diffusion at the cathode side. Compared with the LFP/VA-Li cell, the VA-LFP/VA-Li cell presents further improved rate performance (Figure 4b). For example, VA-LFP/VA-Li delivers high capacities of 147, 129, and  $112 \text{ mAh g}^{-1}$  at C-rates of 2, 3, and 4C, which are higher than that of the LFP/VA-Li cell ( $116, 97, \text{ and } 88 \text{ mAh g}^{-1}$ ). When the C-rate returns to 0.5C, a high capacity of  $165 \text{ mAh g}^{-1}$  is recovered, indicating good stability during cycling at high current densities. The improved rate performance can be attributed to the fast  $\text{Li}^+$  transport in the micro-channels of the DVAEs, thus leading to lower resistances and lower overpotentials.<sup>[15]</sup>

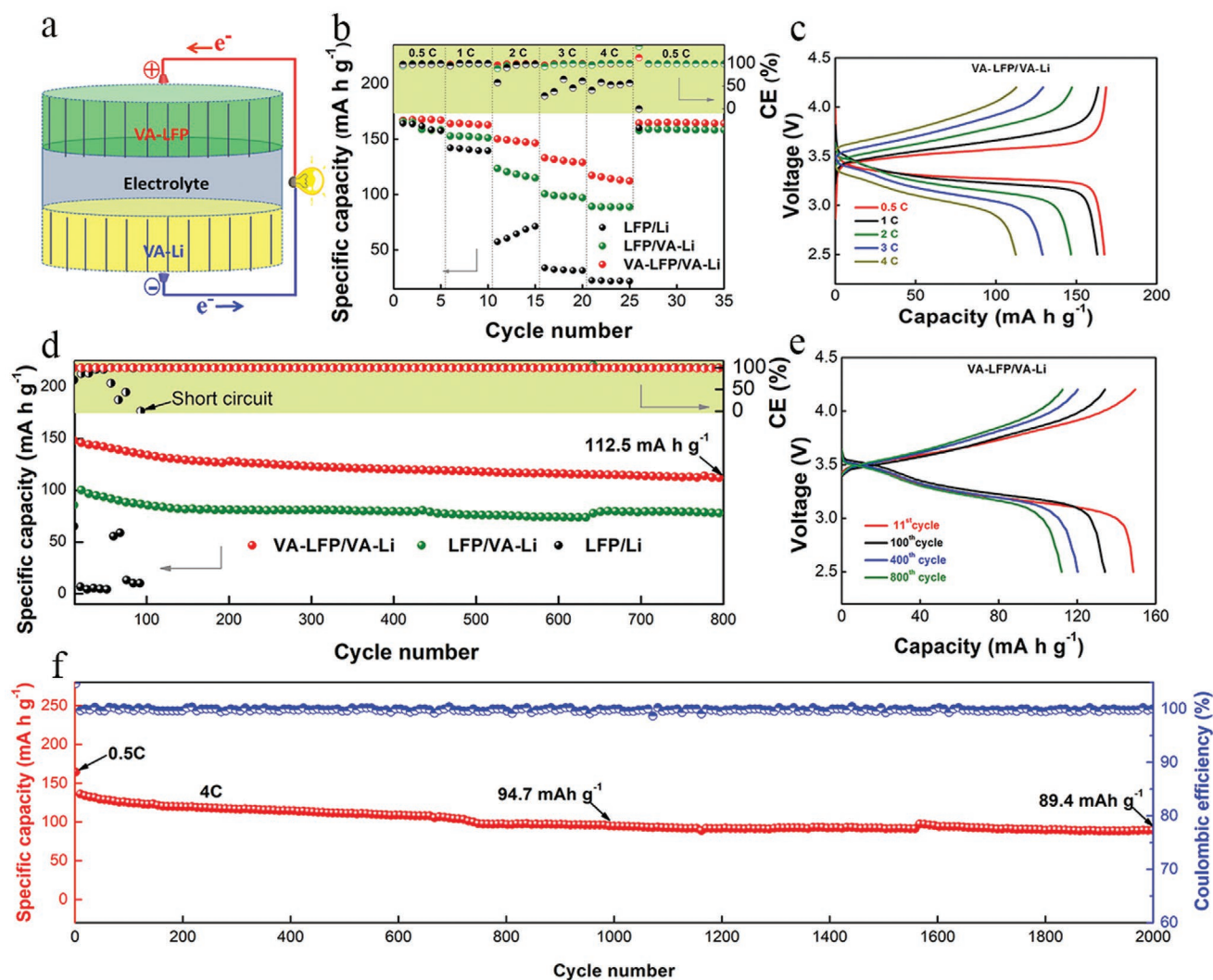


**Figure 4.** Electrochemical performance of fast charging ASSLBs with three different cell configurations (VA-LFP/VA-Li, LFP/VA-Li, and LFP/Li). a) Schematic illustration of VA-LFP cathode and VA-Li anode with SPEs for fast charging ASSLBs. b) LFP/Li, LFP/VA-Li, and VA-LFP/VA-Li full batteries rate performance from 0.5 to 4C. c) Charge and discharge profile of VA-LFP/VA-Li at different rates. d) The cells cycling performance at rate of 2C. e) Charge and discharge profile of VA-LFP/VA-Li at 2C. f) VA-LFP/VA-Li long cycling performance at rate of 4C (LFP loading:  $\approx 2.66 \text{ mg cm}^{-2}$ ).

At 4C, the VA-LFP/VA-Li cell delivers an overpotential of  $\approx 0.66 \text{ V}$  (Figure 4c), which is around 0.1 V smaller than that of the LFP/VA-Li cell (Figure S11, Supporting Information), further confirming the positive effect of VA-LFP on  $\text{Li}^+$  transport.

Besides the rate performance, cycling stability is another important parameter to evaluate suitability for practical application. Hence, the cycling stability of the three cells is further evaluated under a rate of 2C. As shown in Figure 4d, the VA-LFP/VA-Li, LFP/VA-Li, and LFP/Li cells deliver reversible capacities of 148.7, 101.8, and 65.3  $\text{mAh g}^{-1}$  in the initial cycle, respectively. It is noteworthy that a sharp CE drop (indicating the occurrence of short-circuit) is observed after 60 cycles for the LFP/Li cell, while a similar phenomenon does not occur in the LFP/VA-Li and VA-LFP/VA-Li cells. Both of these cells show high cycling stability with capacity retentions greater than 75% after 800 cycles. The results further confirm the strong capability of VA-Li in suppressing Li dendrite formation. The major

differences between LFP/VA-Li and VA-LFP/VA-Li are focused on capacity output and overpotential. As shown in Figure 4d,e and Figure S12 (Supporting Information), after 800 cycles, the VA-LFP/VA-Li exhibits a capacity of 112.5  $\text{mAh g}^{-1}$  and an overpotential of 0.42 V, while a lower capacity of 78.0  $\text{mAh g}^{-1}$  and larger overpotential of 0.63 V are delivered by its counterpart. Considering the same anode and electrolyte used in the two cells, the different electrochemical performance can be attributed to the fast  $\text{Li}^+$  transport in the VA-LFP cathode.

As previously mentioned, in order to meet the requirement of fast charging ALLSBs, a high C-rate of 3.2C is essential. With this in mind, the cycling stability of the VA-LFP/VA-Li cell operating at 4C is studied. As shown in Figure 4d, after 5 activation cycles at 0.5C, an initial capacity of 137.5  $\text{mAh g}^{-1}$  can be achieved at 4C. Even after 2000 cycles, the cell still maintains a capacity of 89.4  $\text{mAh g}^{-1}$ , providing excellent cycling stability. Overall, the proposed DVAEs design for ASSLBs can

remarkably improve the cycling stability and rate-performance through optimizing Li<sup>+</sup> transport and suppressing Li dendrites. This work is of great significance for paving the way toward the application of fast charging ASSLBs.

### 3. Conclusion

In summary, we have developed a strategy using DVAEs to address the issues of poor Li<sup>+</sup> kinetics and dendrite formation in fast charging ASSLBs. On the anode side, the lithiophilic properties of the VA-Li electrode are able to guide the selective nucleation and growth of Li on the micro-walls, filling the void space between the channels and preventing perpendicular growth of dendrites. Moreover, due to the reduced tortuosity for Li<sup>+</sup> transport induced by the vertically-aligned structure in both VA-Li and VA-LFP, the Li<sup>+</sup> transport kinetics are significantly improved. With this in mind, the DVAE design has the potential to enable the fast charging ASSLBs with enhanced electrochemical performance. The high rate capabilities enabled by this design are proven through evaluation of electrochemical performances in Li–Li symmetric cells and Li-LFP full cells. Accordingly, the Li–Li symmetric cell assembled with the VA-Li electrode is able to achieve a long cycle life of 300 h at an ultrahigh current density/areal capacity of 3 mA cm<sup>-2</sup>/3 mAh cm<sup>-2</sup>. To the best of our knowledge, these are the highest values in terms of current density and areal capacity in SPE systems. Additionally, the Li-LFP cell assembled with DVAEs maintains a high capacity of 89.4 mAh g<sup>-1</sup> at 4C after 2000 cycles. This work provides a new strategy for designing fast charging ASSLBs via rational structural design of electrodes.

### Supporting Information

Supporting Information is available from the Wiley Online Library or from the author.

### Acknowledgements

This research was supported by the Natural Science and Engineering Research Council of Canada (NSERC); the Canada Research Chair Program (CRC); and the Canada Foundation for Innovation (CFI), and Western University. X.G. and J.L. acknowledge the financial supported by the Chinese Scholarship Council to conduct research at the University of Western Ontario.

### Conflict of Interest

The authors declare no conflict of interest.

### Author Contributions

X.G., X.Y., and K.A. contributed equally to this work. They conceived the idea and designed the experiments. X.S. and T.-K.S. as supervisors gave guidance and discussion to the project. J.L. and X.G. did the Scanning Electron Microscope (SEM). Q.S. and Y.Z. helped design and discussed the experiments. R.L. assisted with characterizations. All authors discussed the results and commented on the manuscript.

### Keywords

dual vertically-aligned electrodes, fast charging batteries, lithium batteries, lithium dendrite suppression

Received: June 25, 2020

Revised: July 28, 2020

Published online:

- [1] a) X. Yang, J. Luo, X. Sun, *Chem. Soc. Rev.* **2020**, *49*, 2140; b) Y. Kato, S. Hori, T. Saito, K. Suzuki, M. Hirayama, A. Mitsui, M. Yonemura, H. Iba, R. Kanno, *Nat. Energy* **2016**, *1*, 16030; c) Y. Li, J. Fan, J. Zhang, J. Yang, R. Yuan, J. Chang, M. Zheng, Q. Dong, *ACS Nano* **2017**, *11*, 11417; d) Y. Xiao, Y. Wang, S.-H. Bo, J. C. Kim, L. J. Miara, G. Ceder, *Nat. Rev. Mater.* **2020**, *5*, 105; e) X. Yang, X. Li, K. Adair, H. Zhang, X. Sun, *Electrochem. Energy Rev.* **2018**, *1*, 239; f) E. Umeshbabu, B. Zheng, Y. Yang, *Electrochem. Energy Rev.* **2019**, *2*, 199.
- [2] a) X. Yu, L. Wang, J. Ma, X. Sun, X. Zhou, G. Cui, *Adv. Energy Mater.* **2020**, *10*, 1903939; b) S.-J. Tan, X.-X. Zeng, Q. Ma, X.-W. Wu, Y.-G. Guo, *Electrochem. Energy Rev.* **2018**, *1*, 113; c) Q. Zhao, S. Stalin, C.-Z. Zhao, L. A. Archer, *Nat. Rev. Mater.* **2020**, *5*, 229; d) A. Du, H. Zhang, Z. Zhang, J. Zhao, Z. Cui, Y. Zhao, S. Dong, L. Wang, X. Zhou, G. Cui, *Adv. Mater.* **2019**, *31*, 1805930.
- [3] a) J. Wan, J. Xie, X. Kong, Z. Liu, K. Liu, F. Shi, A. Pei, H. Chen, W. Chen, J. Chen, *Nat. Nanotechnol.* **2019**, *14*, 705; b) S.-S. Chi, Y. Liu, N. Zhao, X. Guo, C.-W. Nan, L.-Z. Fan, *Energy Storage Mater.* **2019**, *17*, 309; c) X. Yang, X. Gao, C. Zhao, Q. Sun, Y. Zhao, K. Adair, J. Luo, X. Lin, J. Liang, H. Huang, *Energy Storage Mater.* **2020**, *27*, 198; d) T. Dong, J. Zhang, G. Xu, J. Chai, H. Du, L. Wang, H. Wen, X. Zang, A. Du, Q. Jia, *Energy Environ. Sci.* **2018**, *11*, 1197; e) C. Ma, K. Dai, H. Hou, X. Ji, L. Chen, D. G. Ivey, W. Wei, *Adv. Sci.* **2018**, *5*, 1700996; f) D. Lin, W. Liu, Y. Liu, H. R. Lee, P.-C. Hsu, K. Liu, Y. Cui, *Nano Lett.* **2016**, *16*, 459.
- [4] a) X. Yang, M. Jiang, X. Gao, D. Bao, Q. Sun, N. Holmes, H. Duan, S. Mukherjee, K. Adair, C. Zhao, *Energy Environ. Sci.* **2020**, *13*, 1318; b) Y. Zhang, R. Chen, S. Wang, T. Liu, B. Xu, X. Zhang, X. Wang, Y. Shen, Y.-H. Lin, M. Li, L.-Z. Fan, L. Li, C.-W. Nan, *Energy Storage Mater.* **2020**, *25*, 145; c) W. He, Z. Cui, X. Liu, Y. Cui, J. Chai, X. Zhou, Z. Liu, G. Cui, *Electrochim. Acta* **2017**, *225*, 151; d) X. Zhang, S. Wang, C. Xue, C. Xin, Y. Lin, Y. Shen, L. Li, C. W. Nan, *Adv. Mater.* **2019**, *31*, 1806082.
- [5] a) X. Yang, Q. Sun, C. Zhao, X. Gao, K. Adair, Y. Zhao, J. Luo, X. Lin, J. Liang, H. Huang, *Energy Storage Mater.* **2019**, *22*, 194; b) W. Zhang, J. Nie, F. Li, Z. L. Wang, C. Sun, *Nano Energy* **2018**, *45*, 413; c) F. Chen, D. Yang, W. Zha, B. Zhu, Y. Zhang, J. Li, Y. Gu, Q. Shen, L. Zhang, D. R. Sadoway, *Electrochim. Acta* **2017**, *258*, 1106; d) K. Pan, L. Zhang, W. Qian, X. Wu, K. Dong, H. Zhang, S. Zhang, *Adv. Mater.* **2020**, *32*, 2000399; e) X. Zhong, J. Tang, L. Cao, W. Kong, Z. Sun, H. Cheng, Z. Lu, H. Pan, B. Xu, *Electrochim. Acta* **2017**, *244*, 112; f) Q. Lu, Y. B. He, Q. Yu, B. Li, Y. V. Kaneti, Y. Yao, F. Kang, Q. H. Yang, *Adv. Mater.* **2017**, *29*, 1604460; g) H. Duan, Y.-X. Yin, Y. Shi, P.-F. Wang, X.-D. Zhang, C.-P. Yang, J.-L. Shi, R. Wen, Y.-G. Guo, L.-J. Wan, *J. Am. Chem. Soc.* **2018**, *140*, 82.
- [6] X. Yang, Q. Sun, C. Zhao, X. Gao, K. R. Adair, Y. Liu, J. Luo, X. Lin, J. Liang, H. Huang, *Nano Energy* **2019**, *61*, 567.
- [7] G. G. Eshetu, X. Judez, C. Li, O. Bondarchuk, L. M. Rodriguez-Martinez, H. Zhang, M. Armand, *Angew. Chem., Int. Ed.* **2017**, *56*, 15368.
- [8] a) X. B. Cheng, C. Z. Zhao, Y.-X. Yao, H. Liu, Q. Zhang, *Chem* **2019**, *5*, 74; b) X. Gao, X. Yang, K. Adair, X. Li, J. Liang, Q. Sun, Y. Zhao, R. Li, T. K. Sham, X. Sun, *Adv. Energy Mater.* **2020**, *10*, 1903753.

- [9] a) H. Wang, Y. Liu, Y. Li, Y. Cui, *Electrochem. Energy Rev.* **2019**, *2*, 509; b) J. Lu, Z. Chen, F. Pan, Y. Cui, K. Amine, *Electrochem. Energy Rev.* **2018**, *1*, 35.
- [10] Y. Liu, Y. Zhu, Y. Cui, *Nat. Energy* **2019**, *4*, 540.
- [11] a) S. Deville, *Adv. Eng. Mater.* **2008**, *10*, 155; b) X. Gao, X. Yang, Q. Sun, J. Luo, J. Liang, W. Li, J. Wang, S. Wang, M. Li, R. Li, *Energy Storage Mater.* **2020**, *24*, 682; c) L. Zhou, S. Zhai, Y. Chen, Z. Xu, *Polymers* **2019**, *11*, 712; d) C. Wang, X. Chen, B. Wang, M. Huang, B. Wang, Y. Jiang, R-S Ruoff, *ACS Nano* **2018**, *12*, 5816; e) Y. Yu, H. Zhang, X. Yang, J. Gou, X. Tong, X. Li, H. Zhang, *Energy Storage Mater.* **2019**, *19*, 88.
- [12] a) Y. Zhang, W. Luo, C. Wang, Y. Li, C. Chen, J. Song, J. Dai, E. M. Hitz, S. Xu, C. Yang, Y. Wang, L. Hu, *Proc. Natl. Acad. Sci. USA* **2017**, *114*, 3584; b) C. Sun, Y. Li, J. Jin, J. Yang, Z. Wen, *J. Mater. Chem. A* **2019**, *7*, 7752.
- [13] J. Deng, C. Bae, A. Denlinger, T. Miller, *Joule* **2020**, *4*, 511.
- [14] a) Y. Liu, B. Xu, W. Zhang, L. Li, Y. Lin, C. Nan, *Small* **2019**, *16*, 1902813; b) R. Hu, H. Qiu, H. Zhang, P. Wang, X. Du, J. Ma, T. Wu, C. Lu, X. Zhou, G. Cui, *Small* **2020**, *16*, 1907163.
- [15] a) X. Gao, X. Yang, M. Li, Q. Sun, J. Liang, J. Luo, J. Wang, W. Li, J. Liang, Y. Liu, *Adv. Funct. Mater.* **2019**, *29*, 1806724; b) X. Liang, C. Hart, Q. Pang, A. Garsuch, T. Weiss, L. F. Nazar, *Nat. Commun.* **2015**, *6*, 5682; c) M. K. Song, E. J. Cairns, Y. Zhang, *Nanoscale* **2013**, *5*, 2186.